Chemical Physics Letters 648 (2016) 161–165

Contents lists available at ScienceDirect

Chemical Physics Letters

journal homepage: www.elsevier.com/locate/cplett

Mechanisms of monovacancy diffusion in graphene

Jack D. Wadey[a], Alexander Markevich[a], Alex Robertson[b], Jamie Warner[b], Angus Kirkland[b], Elena Besley[a,*]

[a] School of Chemistry, University of Nottingham, University Park, Nottingham NG7 2RD, UK
[b] Department of Materials, University of Oxford, Parks Road, Oxford OX1 3PH, UK

ARTICLE INFO

Article history:
Received 18 December 2015
In final form 2 February 2016
Available online 10 February 2016

ABSTRACT

A comprehensive investigation of monovacancy diffusion in graphene has been carried out with the use of density functional theory and the climbing image nudged elastic band method. An out-of-plane spiro structure is found for the first-order saddle point, which defines the transition state in the vacancy diffusion pathway. The obtained activation energy for diffusion is significantly lower than the reported values for the in-plane saddle point structures. The time between consecutive vacancy jumps in graphene is estimated to be in the range of 100–200 s at room temperature in a good agreement with experimental observations.

1. Introduction

The intrinsic lattice defects can significantly alter electronic, magnetic and mechanical properties of graphene [1,2]. Understanding the dynamic behaviour of these defects is therefore crucial for controlling and development of desirable graphene properties for different technological applications.

A graphene monovacancy (MV) has been the focus of many theoretical investigations as the logical starting point for studying the more extended vacancy defects [3–14]. After the removal of a C atom from the hexagonal graphene lattice the resulting vacancy, having three dangling bonds, acquires D_{3h} symmetry. Upon structural relaxation, MV undergoes a spontaneous Jahn–Teller distortion lowering the symmetry to C_{2v} and forming both five and nine membered rings. This occurs as two of the undercoordinated C atoms form a weak reconstructed bond with a length of about 1.9–2.0 Å, which is significantly longer than a typical C—C bond in graphene. The resulting structure is referred to as a 5–9 MV. The 5–9 vacancies can be rearranged rapidly to form differently orientated reconstructed bonds around the vacancy. The barrier for this reorientation of the reconstructed bond has been predicted to be 0.17–0.23 eV, with the saddle point structure being the symmetrical (D_{3h}) graphene MV [4,14].

Despite the large amount of published data on graphene MV, there is a discrepancy in the results for the diffusion barrier and saddle point structure, with barriers ranging from 1.0 eV to 1.7 eV and two main saddle point configurations reported [9,14]. Figure 1 shows the migration of a single vacancy in graphene, where a and d are the initial and final positions of the 5–9 vacancy. The two saddle point configurations, shown in Figure 1b and c, have been widely reported in previous theoretical works [3–7,9–12,14]. In these configurations, all C atoms are positioned in the plane of graphene. Figure 1b shows the migrating C atom travelling symmetrically across, whereas in Figure 1c the C atom moves to one side of the vacancy. These structures will be referred to as symmetric and asymmetric saddle point configurations (*s*-SP and *a*-SP, respectively).

Experimental data on the activation barriers for MV diffusion in graphene are absent. However, it is generally assumed that the mechanisms of MV diffusion in graphene and the basal plane of graphite are similar. Early experimental investigations of irradiation induced defects in graphite suggested an activation energy for MV diffusion of 3.1 ± 0.2 eV [15]. However Telling et al. reported that this barrier could be caused by more complex defects and vacancy trapping leading to the higher activation energy [16]. More recently, Asari et al. published Raman measurements of the relaxation processes in ion irradiated graphite and suggested that vacancy migration had an associated barrier of 1.8 ± 0.3 eV [17]. In experimental work by Paredes et al. scanning tunnelling microscopy was used for observations of vacancy diffusion on the surface of graphite. From the observed frequency of vacancy jumps the activation energy for MV diffusion was determined as 0.9–1.0 eV using a pre-exponential factor of $\nu_0 \sim 10^{13}$ s^{-1} for graphite [18].

The more recent experimental results by Asari et al. and Paredes et al. have a closer agreement with the theoretical predictions.

* Corresponding author.
E-mail address: elena.besley@nottingham.ac.uk (E. Besley).

http://dx.doi.org/10.1016/j.cplett.2016.02.005
0009-2614/

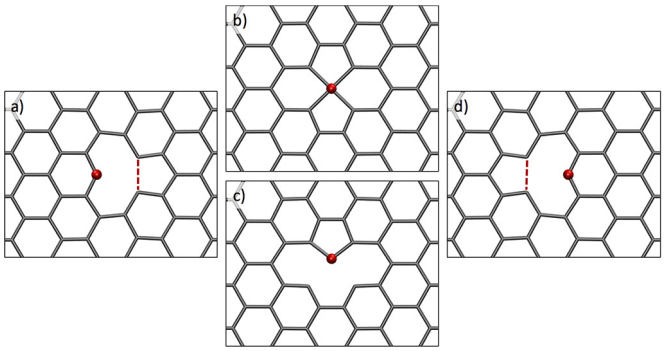

Figure 1. Migration of the MV in graphene: (a) and (d) show initial and final configurations; (b) and (c) are symmetric and asymmetric saddle point structures (*s*-SP and *a*-SP, respectively). All of the C atoms are in-plane, the red C atom is the migrating atom and the reconstructed bond is shown as a red dashed line. (For interpretation of the references to colour in this figure legend, the reader is referred to the web version of this article.)

However, considering the observed frequency of MV diffusion, none of the existing published activation energies can match experimental lifetimes at room temperature, with some having to raise the temperature to achieve reasonable results [5], and others with higher barriers suggesting that MV diffusion would rarely occur at room temperature [6,11,14].

The main focus of this work is to present a thorough overview of monovacancy diffusion in graphene and determine which saddle point structure is the most favourable transition state for diffusion. By studying not only the transition state but also the diffusion profile a greater understanding of vacancy migration is gained. The obtained results are in agreement with the recent experimental work by Robertson et al. [19], where aberration-corrected transmission electron microscopy (AC-TEM) was used to image the MV defect. The authors observed both the 5–9 reconstructed MV structure and the symmetric MV defects, together with the diffusion of the MV. The barrier for diffusion presented here is currently the only theoretical value which is consistent with the experimental observations of the frequency of vacancy jumps at room temperature.

2. Computational methods

All calculations in the present work were performed using the DFT AIMPRO code [20] with periodic boundary conditions (PBC). The exchange-correlation energy was approximated by both the local density approximation (LDA) formulated by Perdew and Wang (PW92) [21] and the generalised gradient approximation (GGA) by Perdew, Burke and Ernzerhof (PBE96) [22].

An uncontracted basis set of atom-centred Gaussian orbitals was used as a part of the AIMPRO formalism. The basis functions are labelled by multiple orbital symbols, where the number of symbols represents the number of different exponents in the basis. The *p* exponent has 4 functions and *d* has 10 functions, therefore the basis set used in this work to describe C atoms, *pdpp*, has 22 functions with 4 different exponents. Core electrons were replaced by norm-conserving pseudopotentials based on the Hartwigsen–Goedecker–Hutter (HGH) scheme [23]. The charge-density was Fourier transformed and fitted using plane waves with a kinetic energy cutoff of 400 hartrees.

Calculations with different sized supercells were made to determine the effect of the intraplane interaction between vacancy defects on the formation energy of the MV, the activation energy for its migration and on the electronic structure. It was found that the 8×8 hexagonal supercell minimised the intraplane interaction due to size constraints at a reasonable computational expense. Brillouin zone sampling was achieved by the Monkhorst–Pack method [24] using a grid of $12 \times 12 \times 1$ *k*-points. The hexagonal lattice parameters to minimise the total energy for pure graphene where found to be $a = 2.445$ Åfor LDA, and $a = 2.468$ Åfor PBE, where c (>15 Å) was sufficiently large to ensure no interplane interactions.

The formation energy of the MV was calculated using the following equation:

$$E_f = E_d + \mu - E_p \tag{1}$$

where E_d and E_p are the energies of the defective and perfect systems, respectively, and μ is the chemical potential calculated as the total energy per atom in graphene.

The nudged elastic band (NEB) method [25] was used to investigate the diffusion profile for the migration of the MV in graphene. NEB uses a force projection scheme to generate a set of 'images' between initial and final states of the system and then relaxes them to the minimum energy pathway (MEP). Climbing image NEB (CI-NEB) [26] was used in most NEB calculations to find the saddle point structure. The CI-NEB method retains the shape of the MEP, but also obtains a thorough convergence to the saddle point.

The time between consecutive jumps of the MV, τ, can be estimated using the Arrhenius equation:

$$\frac{1}{\tau} = A \exp\left[-\frac{E_a}{k_B T}\right] \tag{2}$$

where A is the pre-exponential factor, E_a is the activation energy, k_B is the Boltzmann constant and T is temperature. Analysis of the local minimum and local maximum on the potential energy surface can be used to find the pre-exponential, or frequency factor, A. This is calculated by the Vineyard formula [27] that has the following form for structures with PBC [28]:

$$A = \frac{\prod_{i=1}^{3N-3} \nu_i^{GS}}{\prod_{i=1}^{3N-4} \nu_i^{TS}} \tag{3}$$

where ν_i^{GS} and ν_i^{TS} are the vibrational modes of the ground state and transition state structures, respectively, and N is the number of atoms. Since one of the $3N - 3$ modes is imaginary for the transition state structure it is not included in the denominator in Eq. (3).

3. Results and discussion

In agreement with previous theoretical studies our calculations show that the ground state atomic configuration of the MV in graphene corresponds to the 5–9 reconstructed structure with a weak bond being formed between two of the C atoms with dangling bonds. Our results on the formation energy, the length of the reconstructed bond and magnetic moment (Table 1) are consistent with the values reported in the literature [5,12,29,30]. It was also found that the in-plane 5–9 vacancy is lower in energy than the configuration where the remaining C atom with the dangling bond is displaced out-of-plane for both LDA and GGA functionals, in agreement with the recent works by Latham et al. [5] and Teobaldi et al. [12].

Table 1
Calculated values of the formation energy E_f, magnetic moment M and the reconstructed bond length R for the MV in graphene.

5–9 MV	LDA	GGA
E_f (eV)	8.02	7.64
M (μ_B)	1.39	1.69
R (Å)	1.87	2.02

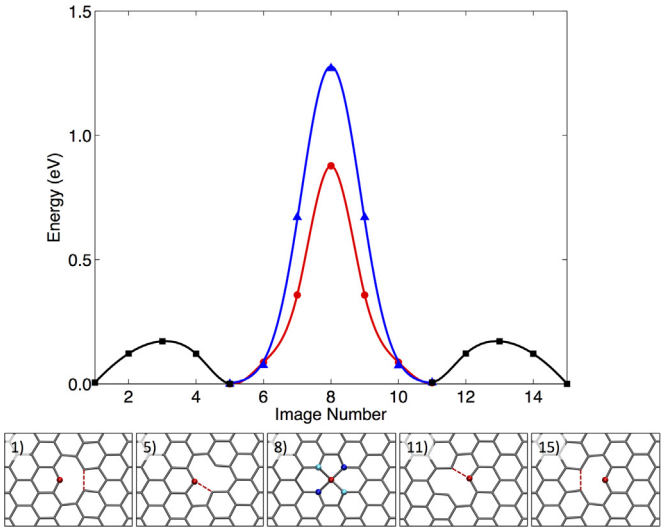

Figure 2. NEB diffusion profiles of the *a*-SP (blue triangles) and NP spiro (red circles) saddle point structures obtained with GGA DFT. Both diffusion profiles undergo a reorganisation, shown by the black line (square points), before the migration. The sequence of images for the NP spiro migration is shown at the bottom. The red C atom is migrating with the reconstructed bond shown by a dashed red line; (1) and (15) are the start and end points, (8) is the NP spiro saddle point structure, (5) and (11) represent the local minima on the profile. (For interpretation of the references to colour in this figure legend, the reader is referred to the web version of this article.)

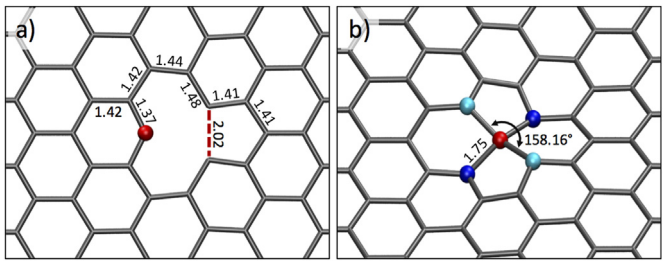

Figure 3. Atomic structures of (a) the 5–9 monovacancy and (b) non-planar (NP) spiro saddle point. The bond length in (a) are shown in Å and obtained from GGA calculations. The red C atom is the migrating atom, the light blue C atoms raised above the graphene plane by 0.33 Å and the dark blue C atoms are displaced below the plane. (For interpretation of the references to colour in this figure legend, the reader is referred to the web version of this article.)

Figure 2 shows the energy profiles along the MV migration pathway obtained from NEB calculations. Image number on the *x* axis corresponds to the images generated by NEB along the diffusion path, with energy on the *y* axis representing an amount (in eV) relative to the minimum energy 5–9 MV structures. It was found that the *a*-SP structure is a transition state for MV migration with an energy barrier of 1.28 eV for GGA and 1.15 eV for LDA. Our calculations also predict a different transition state with a significantly lower energy. The corresponding saddle point structure is shown in Figure 3b, where the migrating atom is positioned in the centre of the compressed tetrahedron with the adjacent C atoms displaced from the graphene plane by 0.33 Å. This lowers the barrier to 0.56 eV for LDA or 0.87 eV for GGA. Table 2 displays the calculated energy barriers for the different saddle point structures, showing that the non-planar (NP) spiro saddle point structure has a lower barrier for both LDA and GGA functionals than the more widely reported structures. For the *s*-SP a separate geometry optimisation was performed since it had not been found from NEB calculations. It should also be noted that calculated energy barriers for the NP spiro saddle point structure are significantly lower than the previously reported barriers for MV diffusion in graphene. A comparison of our results with previous literature is given in Table 3.

Table 2
Activation energies (E_a) for the different saddle point structures calculated with LDA and GGA functionals.

Structure	E_a (eV)	
	LDA	GGA
s-SP	1.23	1.49
a-SP	1.15	1.28
NP Spiro	0.56	0.87

Table 3
Literature DFT results for the migration of the graphene MV. E_a is the activation energy for the migration of the vacancy, with superscript *a* indicating migration towards the edge of the flake and *b* is migration away from the edge. NP is the non-planar spiro structure. Calculations of graphene and graphite used periodic boundary conditions.

System	Method	Reference	E_a (eV)	Structure
Graphene	LDA	[3]	1.01	–
		[4]	1.2	*s*-SP
		[5]	1.24	*a*-SP
	GGA	[4]	1.2	*s*-SP
		[5]	1.25	*a*-SP
		[6]	1.3	*a*-SP
		[7]	1.37	*s*-SP
	DFTB	[6]	1.4	*a*-SP
		[8]	1.29	NP
	TB	[9]	1.0	*s*-SP
		[10]	1.10	*a*-SP
Graphite	LDA	[5]	1.07	*a*-SP
		[11]	1.6	*s*-SP
	GGA	[5]	1.15	*a*-SP
		[7]	1.26	*s*-SP
		[12]	0.99	*s*-SP
C_{116}	B3LYP	[13]	$0.57^a/0.75^b$	NP
$C_{111}H_{26}$	LDA	[14]	1.7	*a*-SP
Graphene	LDA	This Work	0.56	NP
	GGA	This Work	0.87	NP

The graphene sheet is made up of sp^2 hybridised C atoms, resulting in a planar hexagonal lattice with delocalised *p* electrons perpendicular to the plane. When considering the saddle point of the graphene MV, for both the *s*-SP and NP spiro saddle point structures, the migrating C atom is bonded to four other C atoms resulting in sp^3 hybridisation. During the migration, the sp^3 hybridised C atom adopts an out-of-plane structure, thus lowering the energy of the saddle point. This suggests that the NP spiro saddle point would be the more favourable structure over the *s*-SP structure, lowering the activation energy for migration. There have been two suggestions in the literature by both Santana et al. and Zobelli et al. of an out-of-plane saddle point structure. Santana et al. performed calculations on a small graphene flake and found an out-of-plane distortion to the flake [13]. Zobelli et al. reported the same out-of-plane distortion but on graphene with PBC and DFTB. However, their calculated barrier is much larger at 1.29 eV [8].

A theoretical work on the Stone-Wales transformations [31] has shown that instead of the widely reported in-plane rotation of the C—C bond, there is an out-of-plane factor which can alter the transformation mechanism and greatly reduce the activation energy [32]. This also leads to a buckling of the graphene sheet and lowers formation energy of the defect [33]. Both of these papers suggest that an out-of-plane displacements can lower the energy of defects in graphene.

In support of the lower barrier saddle point structure, a vibrational analysis was undertaken to determine the vibrational modes of the three different saddle point structures. The NP spiro structure has just one imaginary vibrational mode, indicating that it is a true

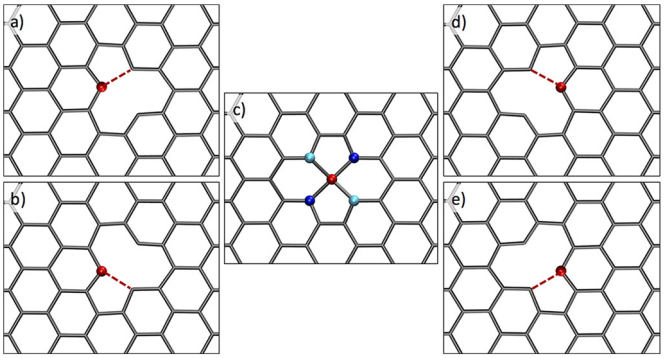

Figure 4. Shorter pathway for vacancy migration with the NP spiro saddle point structure. The red C atom is migrating with the reconstructed bond shown by a dashed red line. (a) and (b) are initial configurations and (d) and (e) are final 5–9 configurations. (For interpretation of the references to colour in this figure legend, the reader is referred to the web version of this article.)

saddle point structure. The *a*-SP structure also has one imaginary mode. On the other hand, the *s*-SP structure has three imaginary modes. These additional imaginary modes indicated both an out-of-plane distortion and a shifting of the central migrating atom towards one side, lowering the symmetry and forming the *a*-SP structure. The analysis of vibrational modes support the results of NEB calculations which show the *a*-SP and the NP spiro structures as transition states for MV migration.

It should also be noted that NEB calculations show the presence of two additional minima along the diffusion profiles, which correspond to different 5–9 MV configurations (Figure 2 images 5 and 11). This indicates that the straight swap migration mechanism actually consists of three independent processes. The first and the last ones correspond to reorganisation between two equivalent 5–9 reconstructions. The energy barrier for this process has been calculated to be 0.17 eV using GGA and 0.23 eV using LDA in a good agreement with the previous studies. The actual migration of the MV, i.e. the change of the lattice position, corresponds to the NEB images from 5 to 11 and involves the motion of one of the C atoms that form the reconstructed bond. The presence of the reorientation steps have also been reported by Hou and Terakura [29] and Zobelli et al. [8]. Taking into account the NP spiro saddle point, the possible pathways for MV diffusion are shown in Figure 4. However, the barrier for reorientation of the reconstructed bond of the 5–9 MV is very small and will not have any effect on the diffusion at room temperature. Therefore, all three C atoms around the MV can be considered to have nearly the same probability to jump to the vacant lattice site.

Figure 4a–e shows the shorter migration mechanism for a vacancy jump, with the lower barrier corresponding to the NP spiro saddle point structure shown in Figure 4c. In reference to Figure 4, the migration can start from a or b, and end with either d or e as once the migrating C atom is in the centre of the vacancy, it should be equally likely to move to either position. Recent theoretical work [10] suggests that vacancies can be attracted to another defect in the graphene sheet. For these vacancies to migrate, it has been suggested that a bond reorganisation of the 5–9 vacancy had to occur. However, using the shorter mechanism, vacancy diffusion can now occur in multiple steps without an intermediate bond reorganisation.

The Vineyard formula [27] (Eq. (3)) was used to calculate the pre-exponential frequency factor, A, in Eq. (2). After diagonalisation of the Hessian matrix (GGA), the products of the vibrational modes for the 5–9 MV, NP spiro and *a*-SP structures were calculated. For the NP spiro structure, $A_{NP} = 1.22 \times 10^{12}\ s^{-1}$, and for the *a*-SP structure, $A_{a\text{-SP}} = 1.11 \times 10^{13}\ s^{-1}$. These results are similar to the estimated frequency factors of 10^{13} or 10^{14} for graphite [18,34]. By substituting the obtained values for the frequency factor into Eq. (2) with the associated barriers for diffusion from Table 2 (GGA), we can estimate the time, τ, between consecutive MV jumps. Taking into account that there are three possible migrating atoms around the MV, τ is estimated to be about 140 s in the case of the NP spiro saddle point and 4.0×10^8 s for the *a*-SP at room temperature. As MV diffusion has been observed experimentally using TEM [19], τ_{NP} is more realistic than $\tau_{a\text{-SP}}$. Using the Arrhenius equation (Eq. (2)) with A_{NP} and $\tau = 1$–200 s (experimental time between vacancy jumps), the activation energy is estimated to have the value of 0.77–0.88 eV, with the calculated barrier for the NP spiro structure within the range.

Table 3 compares our new results for the migration of the MV with previously reported data. Considering systems with PBC, the barriers range from 0.99 eV to 1.6 eV. The most widely reported structure is the *s*-SP structure, but a significant number of papers also report the *a*-SP structure as the favoured configuration. Our calculations in Table 2 find that for both LDA and GGA functionals, the *a*-SP structure has a lower barrier height than the *s*-SP structure. Despite the wide range of theoretical work on the diffusion of the MV, none of the existing barriers in Table 3 are supported by experimental observations for the frequency of MV jumps. At room temperature, the existing theoretical barriers indicate that MV diffusion would be observed rarely, whereas Robertson et al. observe the stable 5–9 MV for 150 s before diffusion occurs [19], supporting our results for the lower activation energy for vacancy diffusion.

4. Conclusions

In the present work mechanisms of monovacancy diffusion in graphene have been investigated with the use of density functional theory. Our calculations show that out-of-plane atomic displacements in the graphene sheet can significantly lower the activation energy for monovacancy migration. A non-planar spiro structure has been found as a transition state for monovacancy migration with an energy barrier of 0.87 eV for GGA and 0.56 eV for LDA. The obtained diffusion barriers are significantly lower than the previously reported values, which are typically in the range of 1–1.3 eV. It is suggested that instead of the widely reported 'straight swap' mechanism, there is a shorter mechanism for vacancy migration where one of the C atoms with the reconstructed bond migrates.

The pre-exponential frequency factor in the Arrhenius law has been calculated with the Vineyard formula using the DFT vibrational modes. A_{NP} ($1.22 \times 10^{12}\ s^{-1}$) with the GGA barrier for diffusion (0.87 eV) was found to closely match the observed frequency of MV diffusion in experiment. Currently, our calculated diffusion barrier is the only barrier with periodic boundary conditions to support the experimental results for MV diffusion at room temperature.

Acknowledgements

E.B. acknowledges an ERC Consolidator Grant for funding. The authors thank the University of Nottingham for access to its high performance computing facility.

References

[1] F. Banhart, J. Kotakoski, A.V. Krasheninnikov, ACS Nano 5 (1) (2011) 26.
[2] A.K. Geim, K.S. Novoselov, Nat. Mater. 6 (2007) 183.
[3] G.D. Lee, C. Wang, E. Yoon, N.M. Hwang, D.Y. Kim, K. Ho, Phys. Rev. Lett. 95 (20) (2005) 205501.
[4] T. Trevethan, C.D. Latham, M.I. Heggie, P.R. Briddon, M.J. Rayson, Nanoscale 6 (5) (2014) 2978.
[5] C.D. Latham, M.I. Heggie, M. Alatalo, S. Oberg, P.R. Briddon, J. Phys.: Condens. Matter 25 (13) (2013) 135403.
[6] A.V. Krasheninnikov, P.O. Lehtinen, A.S. Foster, R.M. Nieminen, Chem. Phys. Lett. 418 (1–3) (2006) 132.

[7] H. Zhang, M. Zhao, X. Yang, H. Xia, X. Liu, Y. Xia, Diamond Relat. Mater. 19 (10) (2010) 1240.
[8] A. Zobelli, V. Ivanovskaya, P. Wagner, I. Suarez-Martinez, A. Yaya, C.P. Ewels, Physica Status Solidi B 249 (2) (2012) 276.
[9] X.H. Xu, C.L. Fu, D.F. Pedraza, Phys. Rev. B 48 (18) (1993) 273.
[10] A.T. Lee, B. Ryu, I.H. Lee, K.J. Chang, J. Phys.: Condens. Matter 26 (11) (2014) 115303.
[11] E. Kaxiras, K.C. Pandey, Phys. Rev. Lett. 61 (23) (1988) 2693.
[12] G. Teobaldi, H. Ohnishi, K. Tanimura, A.L. Shluger, Carbon 48 (14) (2010) 4145.
[13] A. Santana, A.M. Popov, E. Bichoutskaia, Chem. Phys. Lett. 557 (2013) 80.
[14] A. El-Barbary, R. Telling, C. Ewels, M. Heggie, P. Briddon, Phys. Rev. B 68 (14) (2003) 144107.
[15] P.A. Thrower, R.M. Mayer, Physica Status Solidi (A) 47 (1) (1978) 11.
[16] R.H. Telling, C.P. Ewels, A.A. El-Barbary, M.I. Heggie, Nat. Mater. 2 (5) (2003) 333.
[17] E. Asari, M. Kitajima, K.G. Nakamura, T. Kawabe, Phys. Rev. B 47 (17) (1993) 143.
[18] J.I. Paredes, P. Solis-Fernandez, A. Martinez-Alonso, J.M.D. Tascon, J. Phys. Chem. C 113 (2009) 10249.
[19] A.W. Robertson, B. Montanari, K. He, C.S. Allen, Y.A. Wu, N.M. Harrison, A.I. Kirkland, J.H. Warner, ACS Nano 7 (5) (2013) 4495.
[20] P.R. Briddon, R. Jones, Physica Status Solidi B 217 (1) (2000) 131.
[21] J.P. Perdew, Y. Wang, Phys. Rev. B 45 (23) (1992) 244.
[22] J.P. Perdew, K. Burke, M. Ernzerhof, Phys. Rev. Lett. 77 (18) (1996) 3865.
[23] C. Hartwigsen, S. Goedecker, J. Hutter, Phys. Rev. B 58 (7) (1998) 3641.
[24] H.J. Monkhorst, J.D. Pack, Phys. Rev. B 13 (12) (1976) 5188.
[25] G. Henkelman, H. Jonsson, J. Chem. Phys. 113 (22) (2000) 9978.
[26] G. Henkelman, B.P. Uberuaga, H. Jonsson, J. Chem. Phys. 113 (22) (2000) 9901.
[27] G.H. Vineyard, J. Phys. Chem. Solids 3 (1–2) (1957) 121.
[28] A.I. Podlivaev, L.A. Openov, Phys. Solid State 55 (12) (2013) 2592.
[29] Z. Hou, K. Terakura, J. Phys. Chem. C 119 (2015) 4922.
[30] S.T. Skowron, I.V. Lebedeva, A.M. Popov, E. Bichoutskaia, Chem. Soc. Rev. 44 (10) (2015) 3143.
[31] A.J. Stone, D.J. Wales, Chem. Phys. Lett. 128 (5–6) (1986) 501.
[32] A.I. Podlivaev, L.A. Openov, Phys. Lett. A 379 (30–31) (2015) 1757.
[33] S.K. Jain, G.T. Barkema, N. Mousseau, C.M. Fang, M.A. Van Huis, J. Phys. Chem. C 119 (17) (2015) 9646.
[34] F. Banhart, Rep. Prog. Phys. 62 (8) (1999) 1181.